Leon Jampolski[1,*]
Tobias Jakobs[2]
Thomas Kolb[2]
Norbert Willenbacher[1]

Coke Slurries with Improved Higher Heating Value and Good Processability via Particle Shape Design

Coke-water slurries can be used as biogenic intermediates in conversion of residual biomass into high value fuels such as liquefied petroleum gas or synthetic natural gas. The effect of particle size and shape on the flow behavior of slurries including coke particles obtained from fast pyrolysis was investigated. Particles were shaped in a planetary ball mill and equivalent sphere diameter and circularity were used to characterize size and shape. An increased circularity resulted in a strong decrease in slurry viscosity. Accordingly, a higher mass fraction of particles can be mixed into the slurry, thus, increasing the higher heating value while still preserving good processing properties.

Keywords: Coke-water slurry, Particle shape, Particle size distribution, Rheology

Received: February 10, 2017; *revised:* March 17, 2017; *accepted:* June 23, 2017

DOI: 10.1002/ceat.201700061

1 Introduction

Coal-water slurries play an important role in classical energy conversion processes. As the conventional crude oil resources are running low, new opportunities have to be found for producing carbon-based fuels and chemicals. One such possibility could be the bioliq®-process, developed at the Karlsruhe Institute of Technology. Residual biomass, e.g., wheat straw or beech wood, is converted to synthesis gas in a two-step procedure. The first step consists of a fast pyrolysis of the biomass, which is converted into a high-energy-density biogenic intermediate fuel that serves in the second step as feed for high-pressure entrained flow gasification (EFG) to produce synthesis gas [1]. This synthesis gas is treated in a subsequent gas cleaning to obtain high-value products, such as methanol, liquefied petroleum gas (LPG), or synthetic natural gas (SNG) [2].

The solid product of the pyrolysis is coke, which is used in suspensions in subsequent processing steps. The flow behavior of those suspensions has to be controlled carefully for successful and efficient processing. This requires thorough understanding of the effect of particle size (distribution) and shape on suspension rheology. Slurries with carbonaceous solids should have a certain higher heating value (HHV), e.g., to increase the energy output by enhancing the input. Using an aqueous continuous phase, the required HHV can only be reached suspending a high mass and, therefore, volume fraction of coke in such slurries. The particle packing plays an important role to accomplish this challenge.

For spherical particles it is well-known that the maximum packing fraction $\phi_{V_{max}}$ [1)] at which viscosity diverges can be increased using bi- or multimodal particle size distributions. Freely flowing suspensions with $\phi_V > 80\,\%$ can be achieved as the finer particles fill the voids between the coarser ones [3]. For bimodal systems at a given total solids content viscosity reaches a minimum for a fine particle fraction of about 30 %. The maximum packing fraction of anisotropic particles is higher than for spheres [4] but little is known about the variation of $\phi_{V_{max}}$ with size distribution and its effect on flow behavior.

Consequently, starting in the early days of rheology, numerous investigations have been performed regarding the effect of anisotropic, non-Brownian particles on the flow behavior of suspensions, including experimental, theoretical, and numerical investigations [5–14]. In general, at a given particle loading, low shear viscosity increases with rising particle anisotropy.

Prior work with carbonaceous solids suspended in fluids mainly focused on the flow behavior of coal slurries with water or oil as continuous phase. Those kinds of fuels were of particular interest as substitute for fuel oil during the oil crisis in the 1970s [15]. The packing of nonporous spherical coal particles in aqueous slurries has been investigated. Based on data for suspensions including coal particles of distinctly different sizes in various mixing ratios, the so-called reachable concentration, i.e., the particle concentration at which an upper viscosity limit

1) List of symbols at the end of the paper.

[1]Leon Jampolski, Dr. Norbert Willenbacher
leon.jampolski@kit.edu
Karlsruhe Institute of Technology (KIT), Institute for Mechanical Process Engineering and Mechanics, Applied Mechanics, Gotthard-Franz-Straße 3, 76131 Karlsruhe, Germany.
[2]Dr. Tobias Jakobs, Prof. Thomas Kolb
Karlsruhe Institute of Technology (KIT), Institute for Technical Chemistry, Gasification Technology, Herrmann-von-Helmholtz-Platz 1, 76344 Eggenstein-Leopoldshafen, Germany.

acceptable for coal slurry processing is reached, could be increased by about 3 %. Particularly low viscosities could be achieved for mixtures with large size ratio (≈ 1:10) [16, 17].

Papachristodoulou and Trass discussed the rheology of coal-oil slurries covering a broad coal range. Flow behavior is Newtonian up to mass fractions of ϕ_m = 30 % and beyond this point it can be described with the Bingham plastic model due to the emerging yield stress. This flow characteristic is a consequence of dominating attractive van der Waals (vdW) interactions among particles. A decrease of the viscosity and yield stress with increasing mean particle size was observed, especially for high solid concentrations as a consequence of the $1/d$ scaling of the stress related to the vdW attraction [18]. Similar trends for yield stress and viscosity were found by Shivaram et al., though biochar was used instead of coal. Lower viscosities at similar solids loading were achieved using polymeric additives (carboxymethylcellulose sodium salt and poly(butadiene-maleic acid) sodium salt), which may be adsorbed on the particle surface, thus, reducing attractive vdW interactions [19].

Several investigations have shown that coal-water slurries exhibit shear thinning flow behavior. Viscosity could be reduced using a certain amount of fine particle content. For further viscosity reduction, different surface-active additives were used as dispersing or wetting agents, thus, an agglomeration of particles could be prevented and an increase of solids loading of the slurry could be achieved due to reduced attractive interactions among particles [20–26].

The effect of particle porosity and shape were not taken into account in those investigations. However, Zhang et al. evaluated the influence of pores in coal particles on the viscosity of coal-water slurries. Dry coal particles (lignite) absorbed water from air filling the pores partially, resulting in sealed pores. The effective particle porosity is reduced through this phenomenon, which results in a lower viscosity at a given solids content. This effect was not observed for activated carbon or coke particles, since the whole pore volumes were filled with the absorbed water [27].

The effect of particle size distribution (PSD) and porosity on flow behavior at different volume fractions was investigated by Boylu et al. Here, the porosity remained constant during treatment in a laboratory-scale ball mill. A viscosity decrease at constant volume fraction and PSD was observed for coal from lower to higher rank. The dependency of coal-water slurry viscosity on particle shape was hypothesized and the sphericity was suggested as shape parameter but no systematic data were presented [28].

He et al. demonstrated that milling of petroleum coke for petroleum coke-oil slurries resulted in an increased viscosity and they attribute this to the decreasing width of the PSD [29]. The particle size was reduced and more isometric particles were obtained by dispersing raw Indian coal in ionic liquids. Microscopic images of the raw coal indicate irregular shapes and rough surfaces but the shape was not analyzed quantitatively [30]. However, it is well-known that particle shape has a significant influence on the flow behavior of suspensions including non-spherical particles.

As the information about the influence of particle shape on flow behavior is rare for coal respectively coke-water slurries, this work focuses on manipulation of the particle shape and its impact on the viscosity in dependency of the shear rate. Therefore, two coke types with different milling properties were systematically studied.

2 Materials and Methods

2.1 Materials and Equations

Coke particles from wheat straw and beech wood were used in this study. Water served as bulk phase, acting as a model fluid for the aqueous pyrolysis condensate. The volumetric equivalent sphere diameter, as a parameter for the particle size, was determined through Fraunhofer diffraction (HELOS H0309, sympatec GmbH, Clausthal-Zellerfeld, Germany). An ultrasonic wet dispersing unit (QUIXEL, sympatec) was applied for dispersing the particles in water. Porosity ε was measured with mercury intrusion porosimetry (AutoPore IV, micromeritics, Norcross, USA) using a powder sample. The characteristic sharp bend in the intrusion curve separates the regime of inter- and intraparticle pores [31]. Determination of the density ρ was done using a pycnometer according to Gay-Lussac (Carl-Roth GmbH, Karlsruhe, Germany).

The mass fraction of the dispersed solid particles ϕ_m is calculated from the mass of the solid m_{solid} and the mass of the liquid phase m_{liquid}:

$$\phi_m = \frac{m_{solid}}{m_{solid} + m_{liquid}} \tag{1}$$

Then, the density of the solid particles ρ_{solid} can be calculated from ϕ_m and the measured densities of the suspension ρ_{susp} and the liquid phase ρ_{liquid}:

$$\rho_{solid} = \frac{\phi_m}{\frac{1}{\rho_{susp}} - \frac{1-\phi_m}{\rho_{liquid}}} \tag{2}$$

Volume fraction ϕ_V of the coke-water slurries was obtained by Eq. (3), where V_{solid} is the volume of the solid, V_{liquid} is the volume of the liquid, and V_{pore} denotes the particle pore volume.

$$\phi_V = \frac{V_{solid} + V_{pore}}{V_{solid} + V_{liquid}} \tag{3}$$

V_{pore} is defined through (4):

$$\varepsilon = \frac{V_{pore}}{V_{solid} + V_{pore}} \tag{4}$$

Substituting Eqs. (4) and (1) into Eq. (3) results in the final equation for calculating ϕ_V:

$$\phi_V = \frac{\frac{1}{\rho_{solid}}\left(1 + \frac{\varepsilon}{1-\varepsilon}\right)}{\frac{1}{\rho_{solid}} + \frac{1-\phi_m}{\phi_m \rho_{liquid}}} \tag{5}$$

with ρ_{solid} as the density of the solid and ρ_{liquid} as the liquid density, assuming that all pores are filled with the liquid.

2.2 Particle Size and Shape Design

A planetary ball mill (PM200, Retsch GmbH, Haan, Germany) was used for manipulation of particle size and shape. Coke-water suspensions with ϕ_m = 25 % particles were mixed 1:1 (mass ratio) with zirconium oxide balls (diameters 5 mm) in two grinding jars with a volume of 125 mL each. The sun wheel speed was set to 600 min^{-1} and the milling time was varied between 0 to 15 min in 5-min steps. After the milling process and extraction of the milling balls the suspensions with the milled particles were centrifuged (Universal 320, Hettich GmbH, Tuttlingen, Germany) at 9000 rpm for 15 min and the remaining particles were dried at 105 °C for 24 h. A change of physicochemical properties was not observed through this particle treatment.

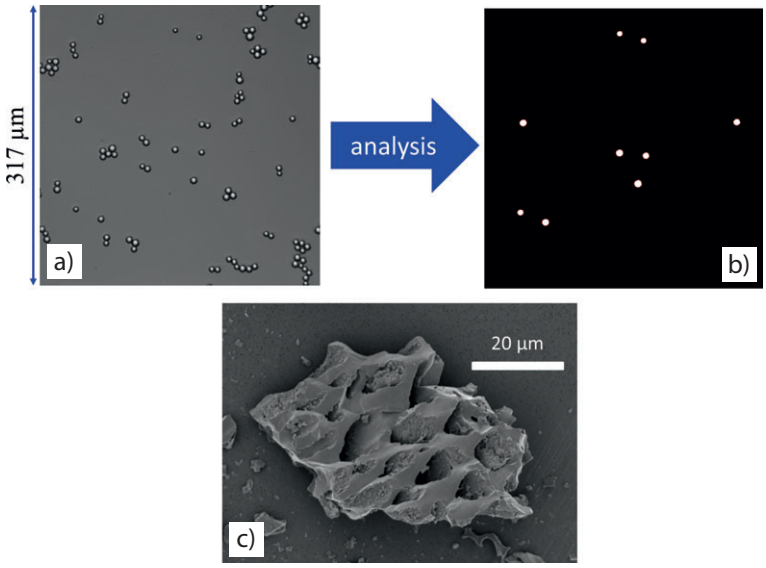

Figure 1. Particle shape analysis. (a) Light microscopy image of SiO_2 particles; (b) image processed using the in-house Matlab scripts; (c) SEM image of a single coke particle.

2.3 Particle Shape Determination

Microscopic images for particle shape determination were taken with an inverse light microscope (Axio Observer D1, Carl Zeiss GmbH, Jena, Germany), equipped with a A-Plan 40×, N.A. 0.65 lens combined with a 1× optovar magnification changer. Images were taken using a sCMOS camera Zyla X (Andor Technology Ltd., Belfast, United Kingdom) with a 21.8 mm diagonal sCMOS sensor size resulting in a maximal size of 2560×2160 pixel. The dimensions of the taken images were 2048×2048 pixel with a resolution of 0.155 µm per pixel for this setup resulting in a side length of 317 µm.

A small amount of particles was dispersed in ethanol using a turbulent beater blade. Afterwards, the suspension was dripped onto a microscope slide. Microscopic images were taken after the ethanol evaporated and the particles were uniformly distributed on the slide. Image analysis was performed using an in-house developed image analyzing tool based on Matlab® (version R2015a, The Mathworks Inc., Natick, MA, USA) scripts. Filters for particle size separation were applied for the detection of agglomerates or too small particles, which appear almost round due to the resolution limits of the taken images. Particles touching the image edges were also eliminated. An example image is shown in Fig. 1.

A light microscopic image of standardized, well-characterized spherical silica particles (Kromasil 100-7-SIL, batch no. 11937, Akzo Nobel, Bohus, Sweden; purchased from MZ-Analysentechnik GmbH, Mainz, Germany) with a nearly monomodal PSD (d_{50} = 6.1 µm) is presented in Fig. 1 a and a typical filtered and contrast-enhanced image is displayed in Fig. 1 b. Several agglomerates were purposely left in the image to demonstrate that the applied filters successfully excluded such agglomerates and only single particles were analyzed. Circularity was chosen as the particle shape parameter since it could be detected with a higher accuracy and reproducibility than the aspect ratio of the coke particles. Circularity not only characterizes the overall particle shape but also accounts for their roughness [32].

Generally, a change in aspect ratio also results in a change in circularity. The definition of circularity C is given in Eq. (6), where A is the detected particle area and P the perimeter of this area. For the spherical silica particles, our image analysis strategy provided a monomodal circularity distribution with $C \approx 1$.

$$C = \frac{4\,\pi A}{P^2} \tag{6}$$

A detailed insight into the irregular shape, roughness, and porosity of the coke particles investigated here is provided by SEM images as exemplarily shown in Fig. 1 c.

2.4 Sample Preparation

Coke particles were slowly mixed into the water using a turbulent beater blade at an angular mixing speed of 200 rpm. An additional stirring period at 400 to 700 rpm, depending on solids content, of 20 min was performed after all particles had been added to the sample to break remaining agglomerates. All rheological measurements were performed right after sample preparation.

2.5 Rheological Characterization

Shear rate-dependent viscosity $\eta(\dot{\gamma})$ measurements were performed using a strain rate controlled rotational rheometer (MARS II, Thermo Fisher Scientific, Karlsruhe, Germany) equipped with a coaxial cylinder geometry (inner diameter 20 mm, outer diameter 21.7 mm) in controlled strain mode. These measurements were conducted using a shear rate ramp (initial shear rate: $\dot{\gamma}_{low}$ = 1 s^{-1}, final shear rate: $\dot{\gamma}_{high}$ = 1000 s^{-1}), holding the shear rate for 30 s or until the measured stress

reached a steady state $(\Delta\sigma/\sigma)/\Delta t < 0.01\,\%\,s^{-1}$ before recording the shear stress and the corresponding viscosity. Preliminary experiments showed that no hysteresis occurred for a shear rate ramp with interchanged initial and final shear rates. All measurements were performed at least three times at a temperature of 20 ± 0.1 °C.

2.6 Intrinsic Viscosity

Determination of the intrinsic viscosity was performed using an Ubbelohde viscometer type I (Schott AG, Mainz, Germany) with an inner capillary diameter of 0.63 mm and a device constant of 0.009869 mm^2s^{-2}. The measurements were conducted in a dilute regime where the relative viscosity η_{rel}, which is the ratio of the suspension viscosity η to the viscosity of the matrix fluid η_{fluid} (see Eq. (7)), depends linearly on ϕ_V (≤ 0.01). Intrinsic viscosity was determined from an extrapolation of $(\eta_{rel} - 1)\phi_V^{-1}$ to $\phi_V = 0$. Standard deviations were calculated from the results of five repeated measurements of each sample. All experiments were performed at 20 ± 0.1 °C.

$$\eta_{rel} = \frac{\eta}{\eta_{fluid}} \tag{7}$$

3 Results and Discussion

3.1 Influence of Milling

Figs. 2 a and c show a sample image of wheat straw coke particles at t_{mill} = 0 min and 15 min, respectively. Comparison indicates the decrease in particle size, also the shape of the milled particles seems smoother than that of the untreated ones. Corresponding images for beech wood coke particles are displayed in Figs. 2 b and d. While a decrease of particle size is clearly visible, a shape change like for the wheat straw coke particles is not obvious from visual inspection. Deeper insight into the effect of milling on the shape of the coke particles is revealed by quantitative image analysis.

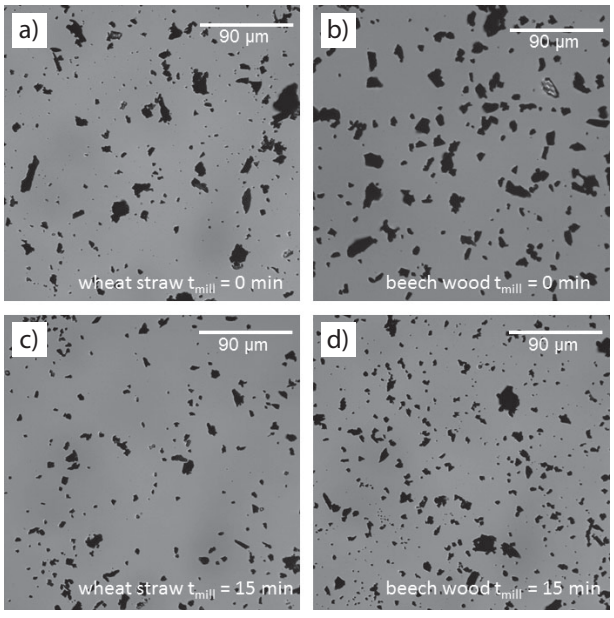

Figure 2. Raw images of wheat straw coke particle at t_{mill} = 0 min (a) and 15 min (c) as well as beech wood coke particles at t_{mill} = 0 min (b) and 15 min (d), qualitatively indicating particle shape and size.

After the described milling procedure, the volumetric equivalent sphere diameter was measured for both coke sorts using Fraunhofer diffraction. Fig. 3 a illustrates the differential and cumulated particle size distributions q_3 and Q_3, respectively, as a function of the particle diameter $d_{particle}$ for wheat straw coke particles. A monotonic decrease of the particle size with increasing milling time is observed and a similar trend is found for beech wood coke particles, as seen in Fig. 3 b.

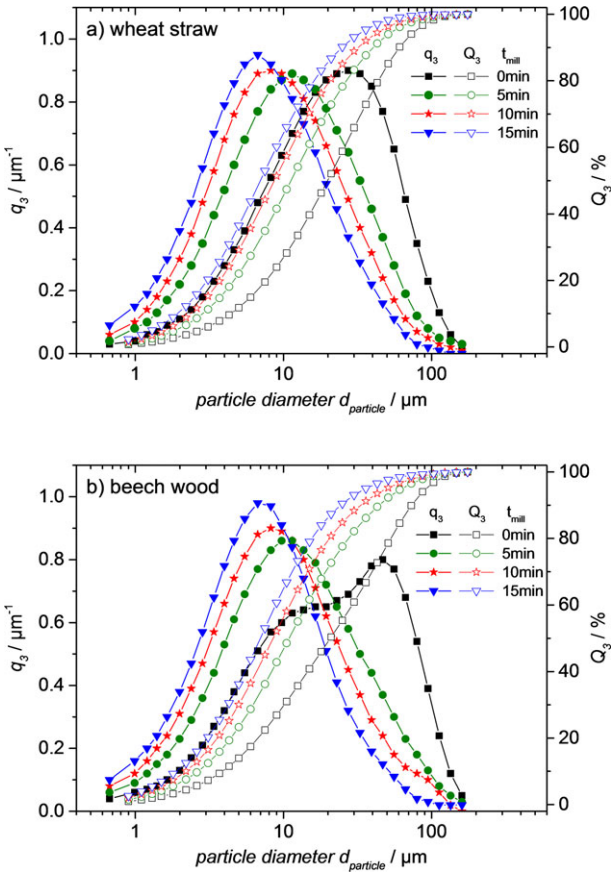

Figure 3. Differential PSD q_3 and cumulated PSD Q_3 as functions of the particle diameter $d_{particle}$ for (a) wheat straw coke and (b) beech wood coke after different milling times in a planetary ball mill.

Both initial samples exhibit a broad PSD but the beech wood powder exhibits a distinct bimodality. This feature vanishes upon milling and for both coke types milling results in a narrower PSD. Tab. 1 summarizes the characteristic particle sizes d_{16}, d_{50}, and d_{84}, PSD width σ_{PSD}, porosity ε, and density ρ_{solid} data together with the corresponding milling times t_{mill}. The median particle diameters of the unmilled coke types were essentially equal ($d_{50} \approx 20$ µm).

Table 1. Characteristic particle sizes at a cumulated PSD of 16 % d_{16}, 50 % d_{50}, 84 % d_{84}, PSD width $\sigma_{PSD} = \ln(d_{84}/d_{16})$, porosity ε, and particle density ρ_{solid} at different milling times for wheat straw and beech wood coke.

	t_{mill} [min]	d_{16} [µm]	d_{50} [µm]	d_{84} [µm]	σ_{PSD} [–]	ε [%]	ρ_{solid} [g cm^{-3}]
Wheat straw	0	6.4	20.0	49.4	2.04	73	1.85
	5	3.9	11.3	31.0	2.07	73	1.85
	10	3.2	8.7	24.1	2.02	73	1.85
	15	2.6	7.0	18.8	1.98	73	1.85
Beech wood	0	5.6	20.8	60.0	2.37	58	1.53
	5	3.7	11.0	32.7	2.18	58	1.53
	10	3.0	8.6	24.2	2.09	58	1.53
	15	2.6	7.0	18.0	1.93	58	1.53

After similar milling time, the equivalent sphere diameters of both coke types were still in the same range, e.g., with a milling time of 15 min the median diameter d_{50} of both samples decreased to 7 µm. Moreover, the d_{16} and d_{84} values are also in the same range. Mercury intrusion porosimetry measurements reveal that the particle porosity is not affected by the grinding procedure even after extended milling. The same is true for the density. Manipulation of particle size in a planetary ball mill provides reproducible results regarding the PSD for both coke feedstocks.

The shape of the particles was analyzed with the method described above using the circularity as characteristic feature. At least 5000 individual particles were analyzed for every particle batch. In Fig. 4, the corresponding differential circularity distributions are shown. The dashed lines indicate the basis splines between the measured points, which fit to the measured data sets. Fig. 4 a displays the circularity distribution of the wheat straw coke particles. A transition from lower to higher circularity with increasing milling time is clearly observed, suggesting a change to a more spherical and smoother particle shape. Fig. 3 b demonstrates the circularity distributions for beech wood coke particles after different milling times. Those curves exhibit no significant change with increasing milling time, indicating that the particle shape remains the same within experimental uncertainty. Comparing the distributions of both coke types at t_{mill} = 0 min indicates that the beech wood coke particles are rounder than the wheat straw coke particles in their original state.

3.2 Influence of Mass and Volume Fraction on Flow Behavior

The viscosity functions for a wheat straw coke slurry (WSCS) with unmilled particles (t_{mill} = 0 min) at different mass, respectively volume fractions (ϕ_m = 10–25 % or ϕ_V = 20.9–56.4 %) are depicted in Fig. 5 a. At low mass fractions, the slurries exhibit Newtonian flow behavior, i.e., the viscosity is constant

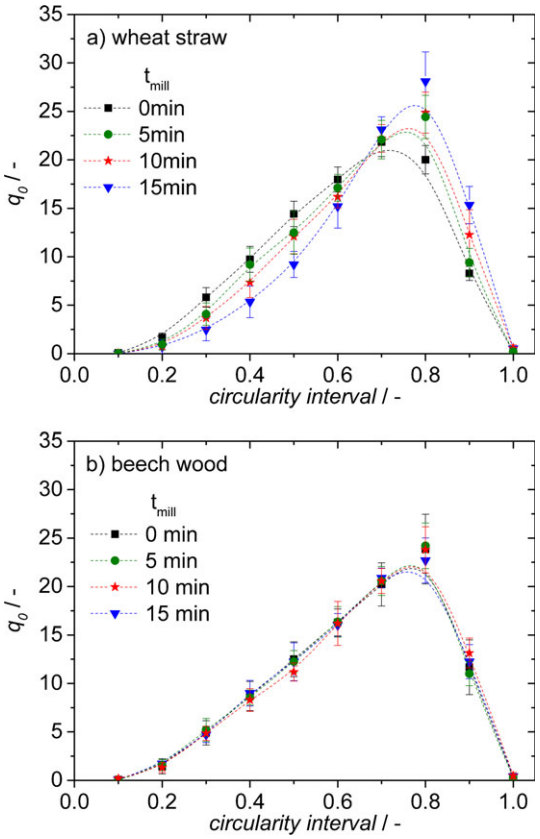

Figure 4. Differential distribution q_0 of circularity after different milling times for (a) wheat straw and (b) beech wood coke. The dashed lines indicate the basis splines between the measured points.

over the whole shear rate range. This constant value is assumed also to be valid for shear rates which could not be measured here. Note, the shear rate range was limited due to the sensitivity of the experimental setup at low shear rates and due to the onset of secondary flows at high shear rates. This Newtonian behavior is common for dilute suspensions of spherical particles ($\phi_V \leq 30$ %) without thermodynamic interactions [33].

With increasing particle loading the flow behavior gets more and more non-Newtonian. A plateau for the zero shear viscosity is not detectable in the investigated shear rate range. Shear-thinning behavior is observed for slurries with mass fractions $\phi_m \geq 12.5$ % ($\phi_V \geq 26.5$ %). The high viscosities at low shear rates are due to interparticle forces like, e.g., vdW forces but with increasing shear rate hydrodynamic forces dominate those particle-particle interactions and a viscosity decrease occurs; also particle orientation in the flow has to be considered. This non-Newtonian flow behavior can be described with the three-parameter Sisko model [34]; see Eq. (8). Here, η is the viscosity, K_S the consistency index, $\dot{\gamma}$ the shear rate, n the flow index, and η_∞ the infinite shear rate viscosity.

$$\eta = K_S \dot{\gamma}^{n-1} + \eta_\infty \tag{8}$$

The Sisko model was already successfully applied to coal-water slurries, although this model does not include a yield

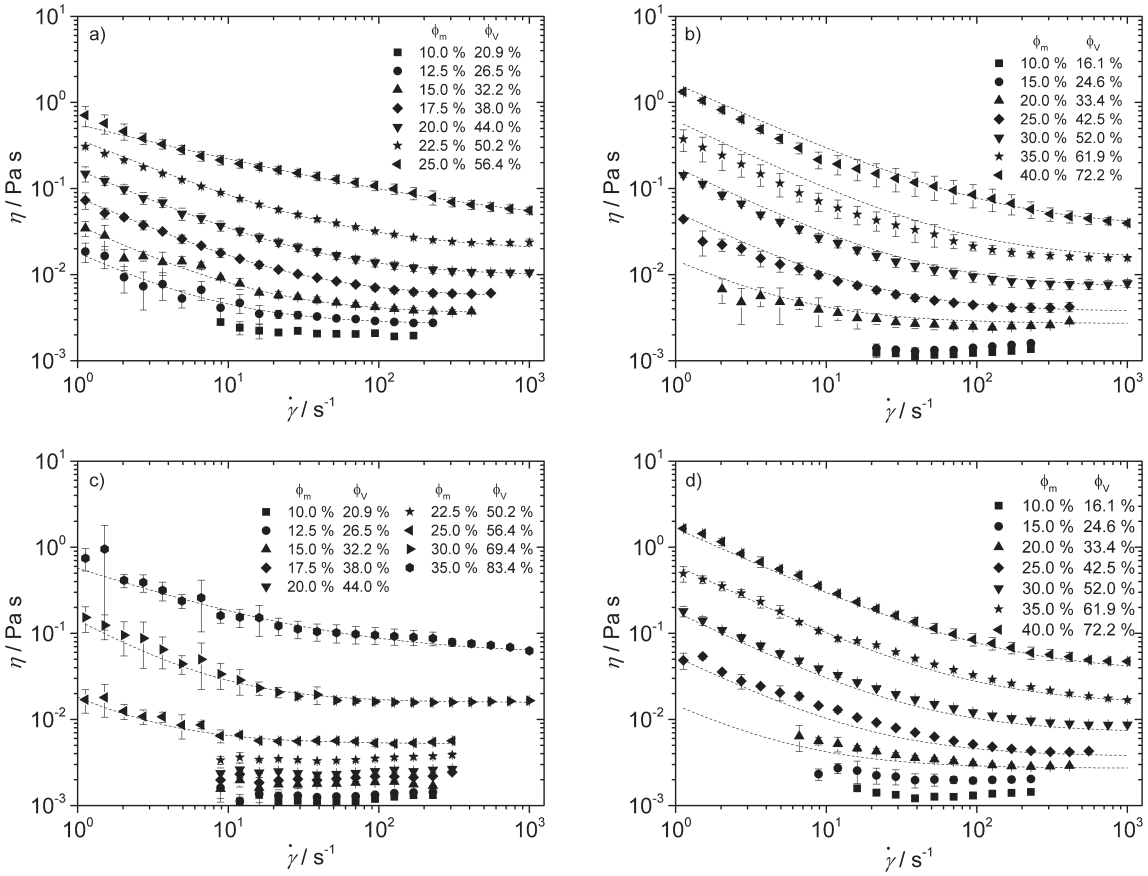

Figure 5. Viscosity η versus shear rate $\dot{\gamma}$ for (a) wheat straw coke slurries (WSCS), (b) beech wood coke slurries (BWCS), both at t_{mill} = 0 min and (c) WSCS, (d) BWCS at t_{mill} = 15 min with different mass and volume fractions. Points are measured values while the dashed lines refer to the fits of the Sisko model to the respective data.

stress parameter. Nevertheless, it describes the flow curves over a wide shear rate range very well [35].

It has to be mentioned that this model does not preclude the presence of a yield stress but just does not cover this aspect of flow behavior. In the case investigated here, a potential yield stress can be estimated to be well below 1 Pa and, thus, it is not relevant for technical processing. Resulting n, K_S and η_∞ values are summarized in Tab. 2 for the four highest volume fractions measured for both slurries at t_{mill} = 0 min and 15 min. The viscosity functions fitted with this model are indicated by the dashed lines through the symbols in all graphs of Fig. 5 for the non-Newtonian flow curves.

In Fig. 5 b, the viscosity functions for a beech wood coke slurry (BWCS) with unmilled particles (t_{mill} = 0 min) at different mass or volume fractions (ϕ_m = 10–40 % or ϕ_V = 16.1–72.2 %), respectively, are illustrated. Viscosity values are quite similar to those obtained for WSCS and non-Newtonian flow behavior sets in at mass fractions $\phi_m \geq 20$ % and data for $\phi_m > 20$ % can also be fitted with the three-parameter Sisko model. For both slurries, non-Newtonian behavior sets in at $\phi_V \approx$ 25–30 %, i.e., at slightly lower ϕ_V values than expected for ideal spherical particles and this is presumably due to the irregular particle shape.

A comparison of WSCS and BWCS with same mass fractions from Figs. 5 a and b reveals that the WSCS has a higher viscosity, especially at high shear rates, than BWCS due to the larger porosity of the wheat straw particles resulting in a higher particle volume fraction for the WSCS at a given mass fraction. The high shear-limiting viscosity η_∞ is independent of thermodynamic particle interactions and solely determined by particle shape and volume fraction.

The viscosity curves at different mass fractions of milled wheat straw particles (t_{mill} = 15 min) are presented in Fig. 5 c. For every mass fraction a significant reduction of the viscosity compared to the corresponding suspension of unmilled particles is observed. This also shows up in the η_∞ data summarized in Tab. 2. This phenomenon is attributed to the increased circularity of the milled wheat straw particles, as the density and porosity remain constant. The influence of the particle shape is discussed in more detail later. Remarkably, using the milled particles it was possible to prepare a suspension with ϕ_m = 35 % with essentially the same viscosity function as the suspension of unmilled particles with ϕ_m = 25 %. The milling step thus turns out to be a valuable tool to increase the energy density of the slurry.

Fig. 5 d exhibits the corresponding viscosity curves of milled beech wood coke (t_{mill} = 15 min) with increasing mass content. In contrast to the WSCS, the BWCS shows minor changes in the viscosity function upon milling comparing Fig. 5 b with

Table 2. Fitting values n, K_S, and η_∞ of the Sisko model for WSCS and BWCS at t_{mill} = 0 and 15 min.

Slurry	ϕ_V [%]	ϕ_m [%]	n [–]	K_S [Pa s^{n-1}]	η_∞ [mPa s]
WSCS, 0 min	38.0	17.5	0.186	0.074	5.4
	44.0	20.0	0.280	0.142	8.9
	50.2	22.5	0.263	0.357	19
	56.4	25.0	0.312	0.788	55.6
WSCS, 15 min	50.2	22.5	–	–	3.6
	56.4	25.0	0.000	0.014	5.2
	69.4	30.0	0.001	0.196	16.2
	83.4	35.0	0.385	0.524	56.6
BWCS, 0 min	42.5	25.0	0.127	0.058	3.8
	52.0	30.0	0.150	0.177	7.4
	61.9	35.0	0.165	0.623	15.4
	72.2	40.0	0.212	1.621	37.3
BWCS, 15 min	42.5	25.0	0.122	0.060	3.6
	52.0	30.0	0.140	0.173	7.7
	61.9	35.0	0.162	0.636	17.1
	72.2	40.0	0.216	1.624	36

Fig. 5 d or the corresponding K_S and η_∞ values in Tab. 2. Minor differences between viscosity functions at the same ϕ_m are presumably due to the differences in the PSD. The suspensions of milled particles with narrower PSD exhibit slightly lower viscosity than suspensions of unmilled particles. The high volume fractions of WSCS with milled particles (up to ϕ_V = 83.4 %) and BWCS (up to ϕ_V = 72.2 %) are enabled by the broad PSD. For monomodal suspensions of spherical particles viscosity diverges at a volume fraction $\phi_{V_{max}}$ = 74 % assuming face-centered cubic packing. Farris demonstrated that the volumetric maximum packing fraction $\phi_{V_{max}}$ is strongly dependent on the PSD and $\phi_{V_{max}}$ > 90 % can be reached for multimodal of very broad PSDs, since the small particles fill the interstitial volume between the bigger particles efficiently [3, 36].

At constant mass fractions, the WSCS still show a higher infinite shear rate viscosity than BWCS with particles which were treated 15 min in the planetary ball mill. However, the flow behavior of WSCS is almost Newtonian for mass fractions up to ϕ_m = 22.5 %, whereas BWCS exhibit a shear-thinning flow behavior starting at a mass fraction of ϕ_m = 20 %. It has to be mentioned that the second Newtonian plateau adjusts faster for the WSCS with milled particles than for the BWCS. As described above, an impact of the particle shape on flow behavior occurs for the WSCS due to milling. In contrast, the flow behavior of BWCS remains constant upon milling since this processing step affects only the particle size but not their shape. This is in common with the findings of Thomas, who investigated suspensions with different particle size and also the matrix fluid viscosity had been varied substantially. No effect of particle size or fluid viscosity on the relative suspension viscosity could be observed [37]. The relative viscosity η_{rel} in Eq. (7) has to be considered as a function of the volume fraction ϕ_V.

Fig. 6 indicates the relative viscosities of untreated WSCS (a) and BWCS (b) suspensions versus volume fraction at various shear rates between 1.1 s^{-1} and 1000 s^{-1}; η values are taken from Fig. 5 and η_{fluid} = 1 mPa s. With increasing shear rate, η_{rel} reduces due to decreasing relevance of thermodynamic particle interactions compared to hydrodynamic forces and due to an alignment of particles in the flow field. The effect of flow alignment on particle packing and flow resistance has been thoroughly discussed by Donev et al. [38].

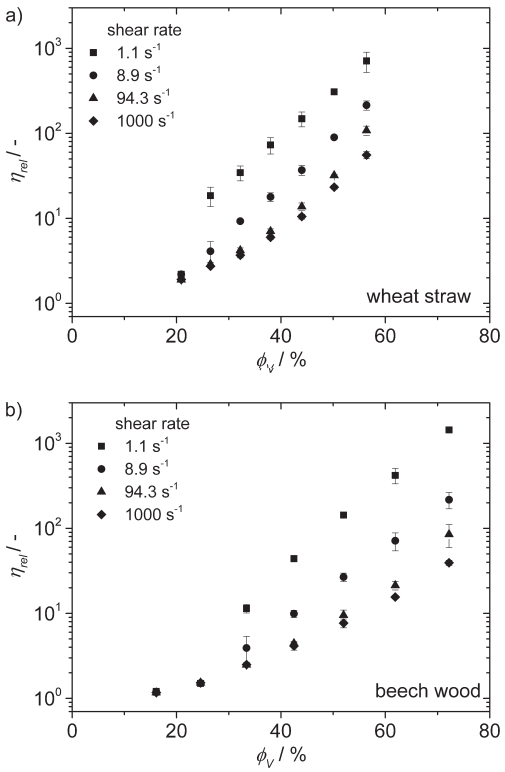

Figure 6. Relative viscosity η_{rel} versus volume fraction ϕ_V at shear rates $\dot{\gamma}$ of 1.1 s^{-1} (square), 8.9 s^{-1} (circle), 94.3 s^{-1} (triangle), and 1000 s^{-1} (diamond) for (a) WSCS and (b) BWCS with untreated particles (t_{mill} = 0 min).

Newtonian flow behavior for the dilute suspensions (ϕ_V < 25 %) implies that the respective η_{rel} data lie in a narrow range. For higher volume fractions, the η_{rel} versus ϕ_V curves obtained at different shear rates diverge reflecting the shear-thinning behavior. Note, for volume fractions ϕ_V > 44 % even the η_{rel} versus ϕ_V curves for the two highest shear rates (94.3 s^{-1} and 1000 s^{-1}) diverge since the second Newtonian plateau is attained at higher shear rates as ϕ_V increases. Observations made for WSCS and BWCS are very similar. However, the non-Newtonian flow behavior starts at higher volume fraction for BWCS than for WSCS, and the same applies for the second Newtonian plateau.

For further investigations regarding the influence of the particle shape on flow behavior, the relative viscosity, taken at shear rates of $\dot{\gamma}_{low} = 1.1\,s^{-1}$ and $\dot{\gamma}_{high} = 1000\,s^{-1}$, will be discussed.

3.3 Influence of Particle Shape on Viscosity in the Low- and High-Shear Regime

Fig. 7 displays the relative viscosity as a function of volume fraction for coke slurries with particles, which were milled for different periods of time. For WSCS (Fig. 7 a), a monotonic decrease of the relative viscosity with increasing milling time of the particles is observed in the low-shear regime as well as in the high-shear regime. Nicoleit et al. made similar observations regarding a decrease of η_{rel} with milled particles, but received a reduced porosity of the wheat straw coke particles due to their grinding setup and, therefore, attributed this reduction in relative viscosity at constant mass fraction to the porosity decrease. However, the particle shape was not taken into account [39].

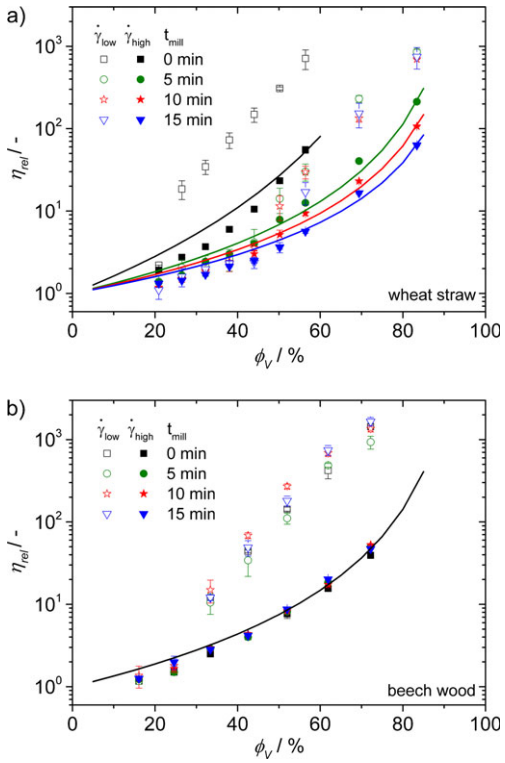

Figure 7. Relative viscosity η_{rel} versus volume fraction ϕ_V at $\dot{\gamma}_{low} = 1.1\,s^{-1}$ and $\dot{\gamma}_{high} = 1000\,s^{-1}$ for (a) WSCS and (b) BWCS made from coke particles milled for different periods of time. The lines indicate fits of the model suggested by Santamaria-Holek and Mendoza keeping the parameter $\phi_{V_{max}}$ constant at $\phi_{V_{max}} = 96\,\%$ and using $[\eta]$ as the only free fit parameter characterizing the change in particle shape upon milling [10].

Here, one can exclude a change in porosity due to milling and hence, the decrease of viscosity is ascribed to the increase in circularity of the particles, as indicated in Fig. 4 a. From a milling time of 0 to 5 min, η_{rel} at $\dot{\gamma}_{low} = 1.1\,s^{-1}$ drops from 710 to 30 at $\phi_V = 56.4\,\%$ which is a reduction by a factor of almost 25. Similar relative viscosity values are found for milling times of 5 and 10 min as expected since the circularity distribution is essentially the same. A further increase in circularity was achieved for $t_{mill} = 15$ min, resulting in a further drop of low shear viscosity to $\eta_{rel} = 17$. At a high shear rate of $1000\,s^{-1}$, the relative viscosity reduces from $\eta_{rel} = 55$ to $\eta_{rel} = 5.6$ for a milling time of 15 min.

The model of Santamaria-Holek and Mendoza was used to describe the dependence of η_{rel} and ϕ_V quantitatively. This model is a modification of the Krieger-Dougherty approach [40], taking the effect of particle shape on intrinsic viscosity $[\eta]$ and maximum packing fraction $\phi_{V_{max}}$ into account [10]. Their expression for the relative viscosity is given in Eq. (9). Here, c is a constant calculated according to Eq. (10).

$$\eta_{rel} = \left(1 - \frac{\phi_V}{1 - c\,\phi_V}\right)^{-[\eta]} \tag{9}$$

$$c = \frac{1 - \phi_{V_{max}}}{\phi_{V_{max}}} \tag{10}$$

This model includes two parameters, namely, the maximum packing fraction $\phi_{V_{max}}$ and the intrinsic viscosity $[\eta]$. The former depends on the PSD as well as on the particle shape, whereas the latter is solely determined by the particle shape. Both parameters are strongly correlated and cannot be fitted simultaneously. Thus, the maximum packing fraction was held constant and determined the intrinsic viscosity $[\eta]$. A value $\phi_{V_{max}} = 96\,\%$ was selected here considering the very broad PSDs for all used coke fractions and assuming that the change of shape relevant here is of minor impact. This assumption seems to be reasonable especially in the high-shear regime where particle alignment is supposed to occur and only those η_{rel}–ϕ_V data sets were fitted. The intrinsic viscosity is, therefore, the only fitting parameter. The resulting values for the averaged intrinsic viscosity values for WSCS are 4.6 ± 0.07, 2.7 ± 0.01, 2.3 ± 0.01, and 2.1 ± 0.01 at milling times of 0, 5, 10, and 15 min. This reduction is consistent with the rising circularity, i.e., increasing roundness and decreasing roughness. The limiting $[\eta]$ value for spheres is 2.5 but for anisotropic particles aligned in strong flow fields even lower values are possible.

In conclusion, the milling step enabled us to increase the particle mass fraction and hence, the HHV of WSCS without increasing the viscosity level, thereby guaranteeing good pumpability and gasification.

In Fig. 7 b, the relative viscosity versus ϕ_V data for BWCS are displayed. In contrast to WSCS no significant change of the η_{rel} versus ϕ_V curves could be achieved by the milling procedure irrespective of milling time. Neither at low nor at high shear rates a measurable effect could be detected as expected, since circularity distribution does not change during milling time of the beech wood coke particles (Fig. 4 b). The porosity and density of the particles also remain constant, and obviously the flow behavior of BWCS does not depend on the particle size in the investigated range. Again setting $\phi_{V_{max}} = 96\,\%$ as for the WSCS, an intrinsic viscosity $[\eta] = 2.8 \pm 0.04$ was obtained from fitting the relative viscosities at $\dot{\gamma} = 1000\,s^{-1}$ independent of

milling time. This is in the same range as the value for $[\eta]$ for WSCS at a milling time of 5 min.

Finally, it should be noted that the intrinsic viscosity data obtained from viscosity measurements according to the fitting procedure described above are in excellent agreement with direct determinations of this quantity from dilute suspension viscosity as obvious from Tab. 3.

Table 3. Values of the intrinsic viscosity $[\eta]$ obtained with an Ubbelohde viscometer from plots of $(\eta_{rel} - 1)\phi_V^{-1}$ against $\phi_V = 0$.

	t_{mill} [min]	$[\eta]$ [–]
Wheat straw	0	4.38 ± 0.02
	15	2.24 ± 0.05
Beech wood	0	2.74 ± 0.10
	15	2.83 ± 0.07

These consistent results including three independent sets of experimental data justify to neglect the effect of circularity on $\phi_{V_{max}}$ allowing for a robust fit of the model described by Eq. (9) to our experimental data. Note that the intrinsic viscosity values below the rigid sphere limit of 2.5 can be rationalized, keeping in mind the high porosity of the particles allowing for a fluid flow inside the particles [41].

4 Conclusions

The influence of particle volume fraction, size, and shape on flow behavior of coke-water slurries was investigated. Two different coke feedstocks, namely, wheat straw and beech wood, with similar initial mean particle diameter were treated in a planetary ball mill. Both coke sorts exhibited an equal reduction in particle size with longer milling time. Additionally, the wheat straw coke particles changed their shape with increasing milling time, quantitatively evaluated by a rising circularity. In contrast, the shape of the beech wood coke particles did not change. In both cases, the particle porosity remained constant irrespective of the milling time.

Slurries including those coke particles were prepared and rheologically characterized. For low mass, respectively volume fractions ($\phi_V \leq 20\,\%$), the suspensions behaved like Newtonian fluids, while for higher particle loadings shear-thinning behavior occurred. The shape of the corresponding viscosity over shear rate curves is mathematically well-described by the Sisko model. For WSCS, the viscosity at constant mass fraction decreased with increasing milling time of particles, which is attributed to the increased circularity. Accordingly, higher mass fraction of particles could be mixed into the slurry, at a selected viscosity level providing good processability. This corresponds to an increased energy density and, thus, HHV of the slurry. In contrast, the BWCS exhibited similar viscosity functions independent of the milling time as their circularity distribution remained unaltered. Porosity and density of both coke feedstocks stayed constant during milling and the particle size decreased in the same manner. Obviously, the particle shape is the relevant parameter controlling the change in flow behavior observed for WSCS.

The effect of particle shape on coke slurry viscosity was captured quantitatively using the model of Santamaria-Holek and Mendoza describing the dependence of relative viscosity on particle volume fraction. This model includes two parameters, namely the maximum packing fraction and the intrinsic viscosity. The former depends on the PSD as well as on particle shape, whereas the latter is solely determined by the particle shape. Accordingly, both parameters are strongly correlated and cannot be fitted simultaneously. Thus, the maximum packing fraction was held constant and the intrinsic viscosity $[\eta]$ was determined from fitting the well-established phenomenological model to our experimental data.

The intrinsic viscosity values obtained that way remained unchanged upon milling for beech wood coke while they decreased for wheat straw coke. This is in line with image analysis results revealing a constant circularity for beech wood coke and an increase of this shape parameter upon milling for wheat straw coke. Moreover, excellent agreement was found of absolute intrinsic viscosity values obtained from modeling the viscosity of concentrated suspensions and those directly obtained from dilute suspension viscometry. This consistent data analysis including three independent measurements justifies this simplified but robust approach suggested here for quantitatively modeling coke slurry viscosity.

These investigations finally provide evidence that the flow behavior of coke-water slurries can be tailored by changing the particle shape. A viscosity reduction can be achieved by milling of wheat straw coke particles enabling a substantially increased particle loading, i.e., HHV at a viscosity level still providing good transport and gasification properties.

Acknowledgment

The authors like to thank the Helmholtz Association of German Research Centers (HGF) for partial funding of the work. Experimental support by Rafael Mayorga Gonzalez and Astrid Huber and providing the coke by Mark Eberhard is gratefully acknowledged.

The authors have declared no conflict of interest.

Symbols used

A	[px^2]	area of projection
c	[–]	constant, see Eq. (10)
C	[–]	circularity
d	[µm]	particle size
$d_{particle}$	[µm]	particle diameter
K_S	[Pa s^{n-1}]	consistency index
m	[g]	mass
n	[–]	flow index
P	[px]	perimeter
Δt	[s]	time difference
t_{mill}	[min]	milling time
V	[cm^3]	volume

Greek letters

$\dot{\gamma}$	[s^{-1}]	shear rate
ε	[%]	porosity
η	[Pa s]	dynamic viscosity
η_{fluid}	[Pa s]	bulk viscosity
η_{rel}	[–]	relative viscosity
η_∞	[mPa s]	infinite shear rate viscosity
$[\eta]$	[–]	intrinsic viscosity
ρ	[g cm^{-3}]	density
σ	[Pa]	shear stress
σ_{PSD}	[–]	width of the PSD
$\Delta\sigma$	[Pa]	shear stress difference
ϕ_m	[%]	mass fraction
ϕ_V	[%]	volume fraction

Subscripts

max	maximal
susp	suspension

Abbreviations

BWCS	beech wood coke slurry
EFG	entrained flow gasification
HHV	higher heating value
LPG	liquefied petroleum gas
PSD	particle size distribution
SNG	synthetic natural gas
vdW	van der Waals
WSCS	wheat straw coke slurry

References

[1] C. Higman, M. Van Der Burgt, *Gasification*, Elsevier, Amsterdam **2003**.
[2] N. Dahmen, E. Henrich, E. Dinjus, F. Weirich, *Energy Sustainability Soc.* **2012**, *2*, 3.
[3] R. J. Farris, *Trans. Soc. Rheol.* **1968**, *12*, 281.
[4] D. A. Weitz, *Science* **2004**, *303*, 968–969.
[5] G. B. Jeffery, *Proc. R. Soc. A* **1922**, *102*, 161–179.
[6] G. I. Taylor, *Proc. R. Soc. London, Ser. A* **1932**, *138*, 41–48.
[7] J. M. Rallison, *J. Fluid Mech.* **1978**, *84*, 237–263.
[8] S. Haber, H. Brenner, *J. Colloid Interface Sci.* **1984**, *97*, 496–514.
[9] H. Brenner, *Int. J. Multiphase Flow* **1974**, *1*, 195–341.
[10] I. Santamaría-Holek, C. I. Mendoza, *J. Colloid Interface Sci.* **2010**, *346*, 118–126.
[11] H. Giesekus, in *Physical Properties of Foods* (Ed: R. Jowitt), Applied Science Publishers, London **1983**, 205–220.
[12] A. B. D. Brown, S. M. Clarke, P. Convert, A. R. Rennie, *J. Rheol.* **2000**, *44*, 221–233.
[13] S. Yamamoto, T. Matsuoka, *Comput. Mater. Sci.* **1999**, *14*, 169–176.
[14] W. Pabst, E. Gregorová, C. Berthold, *J. Eur. Ceram. Soc.* **2006**, *26*, 149–160.
[15] N. Hashimoto, *Coal Prep.* **1999**, *21*, 3–22.
[16] Y. Tu, Z. Xu, W. Wang, *Powder Technol.* **2015**, *281*, 121–128.
[17] X. Yang, Y. Tu, Y. Ren, Z. Xu, *Fuel* **2016**, *168*, 54–60.
[18] G. Papachristodoulou, O. Trass, *Powder Technol.* **1984**, *40*, 353–362.
[19] P. Shivaram, Y. K. Leong, H. Yang, D. K. Zhang, *Fuel* **2013**, *104*, 326–332.
[20] N.-S. Roh, D.-H. Shin, D.-C. Kim, J.-D. Kim, *Fuel* **1995**, *74*, 1220–1225.
[21] Z. Aktaş, E. T. Woodburn, *Fuel Process. Technol.* **2000**, *62*, 1–15.
[22] K. K. Tiwari, S. K. Basu, K. C. Bit, S. Banerjee, K. K. Mishra, *Fuel Process. Technol.* **2004**, *85*, 31–42.
[23] R. Chen, M. Wilson, Y. K. Leong, P. Bryant, H. Yang, D. K. Zhang, *Fuel* **2011**, *90*, 1689–1695.
[24] M. Pawlik, J. S. Laskowski, H. Liu, *Coal Prep.* **1997**, *18*, 129–149.
[25] M. Pawlik, *Colloids Surf., A* **2005**, *266*, 82–90.
[26] R. Xu, W. Zhuang, Q. He, J. Cai, B. Hu, J. Shen, *AIChE J.* **2009**, *55*, 2461–2467.
[27] J. Zhang, H. Zhao, C. Wang, W. Li, J. Xu, H. Liu, *Fuel* **2016**, *177*, 19–27.
[28] F. Boylu, H. Dinçer, G. Ateşok, *Fuel Process. Technol.* **2004**, *85*, 241–250.
[29] Q. He, R. Wang, W. Wang, R. Xu, B. Hu, *Fuel* **2011**, *90*, 2896–2901.
[30] S. Bhoi, T. Banerjee, K. Mohanty, *Fuel Process. Technol.* **2016**, *151*, 1–10.
[31] S. Lowell, J. E. Shields, *Powder Surface Area and Porosity*, Chapman & Hall, London, **1991**.
[32] E. Olson, *J. GXP Compliance* **2011**, *15*, 85–96.
[33] A. B. Metzner, *J. Rheol.* **1985**, *29*, 739.
[34] A. W. Sisko, *Ind. Eng. Chem.* **1958**, 1789–1792.
[35] R. M. Turian, J. F. Attal, D. Sung, L. E. Wedgewood, *Fuel* **2002**, *81*, 2019–2033.
[36] C. Servais, R. Jones, I. Roberts, *J. Food Eng.* **2002**, *51*, 201–208.
[37] D. G. Thomas, *J. Colloid Sci.* **1965**, *20*, 267–277.
[38] A. Donev, I. Cisse, D. Sachs, E. A. Variano, F. H. Stillinger, R. Connelly, S. Torquato, P. M. Chaikin, *Science* **2004**, *303*, 990–993.
[39] T. Nicoleit, N. Dahmen, J. Sauer, *Energy Technol.* **2016**, *4*, 221–229.
[40] I. M. Krieger, T. J. Dougherty, *Trans. Soc. Rheol.* **1959**, *3*, 137–152.
[41] M. A. Nawab, S. G. Mason, *J. Phys. Chem.* **1958**, *62*, 1248–1253.

